2020 SNMMI Highlights Lecture: Cardiovascular Nuclear and Molecular Imaging

Mehran M. Sadeghi, MD, Yale School of Medicine, New Haven, CT

From the Newsline Editor: The Highlights Lecture, presented at the closing session of each SNMMI Annual Meeting, was originated and presented for more than 30 years by Henry N. Wagner, Jr., MD. Beginning in 2010, the duties of summarizing selected significant presentations at the meeting were divided annually among 4 distinguished nuclear and molecular medicine subject matter experts. Each year Newsline publishes these lectures and selected images. The 2020 Highlights Lectures were delivered on July 14 as part of the SNMMI Virtual Annual Meeting. In this issue we feature the lecture by Mehran M. Sadeghi, MD, a professor in the Department of Internal Medicine (Cardiology) at Yale University School of Medicine (New Haven, CT), and Veterans Affairs Connecticut Healthcare System, who spoke on highlights in cardiovascular nuclear and molecular imaging. Note that in the following presentation summary, numerals in brackets represent abstract numbers as published in The Journal of Nuclear Medicine *(2020;61[suppl 1]).*

It is an honor to review some of the best cardiovascular abstracts presented at the 2020 SNMMI Annual Meeting. As in previous years, we saw a large number of cardiovascular abstracts from around the globe. The top 3 contributing countries were the United States, China, and Japan, with 14 other countries represented. Forty-eight abstracts were planned as oral presentations and 53 as posters. Of the 101 total abstracts, 75% were on clinical and 25% on basic and translational science topics. These presentations can be categorized into 3 groups: those focused on refining the practice of nuclear cardiology, those addressing diagnostic gaps and new applications, and those advancing scientific discovery.

The program committee selected 6 abstracts as finalists for the Cardiovascular Council Young Investigator Award (YIA) competition. These finalists included investigators from 3 continents and covered a broad range of topics. I would like to congratulate these authors, who are on their way to being the future leaders of our field. I will be highlighting each of their contributions in different parts of today's lecture. Special recognition goes to Nele Hermanns and Jacek Kwiecinski, MD, who were the Cardiovascular Council YIA winners.

Hermanns et al. from the Hannover Medical School (Germany) reported on "Molecular imaging of inflammation in the brain–heart axis after ischemic stroke: Comparison of 2 murine stroke models" [88]. Stroke is associated with increased risk of myocardial infarction (MI) and cardiac dysfunction, and systemic inflammation is present after stroke. These authors used 2 mouse models of induced stroke: middle cerebral artery occlusion (MCAO) and topical application of a vasoconstrictor, endothelin-1. They used a translocator protein (TSPO)–targeted tracer, ^{18}F-GE180, to image neuroinflammation with whole-body PET, along with MR imaging of the brain and the heart, followed by autoradiography (Fig. 1). Their study showed a larger area of infarct in the MCAO model, which was associated with increased TSPO signal on both PET and autoradiography. The increase in the brain TSPO signal was associated with an increase in the cardiac TSPO signal and a reduction in left ventricular ejection fraction (LVEF) at both 1 and 2 weeks after stroke induction. They noted an inverse relationship between the extent of stroke and LVEF. The authors concluded that their MCAO model enables imaging studies of brain–heart networking after stroke, which evokes elevated TSPO PET signal in both brain and heart, and that "the severity of cerebral ischemic damage may contribute to cardiac dysfunction via systemic inflammation."

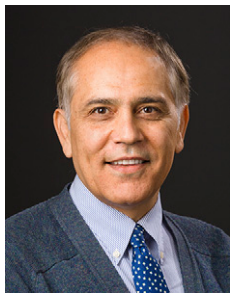

Mehran M. Sadeghi, MD

Kwiecinski et al. from the Institute of Cardiology (Warszawa, Poland), Cedars-Sinai Medical Center (Los Angeles, CA), and the University of Edinburgh (UK) reported on "Clinical predictors of ^{18}F-sodium fluoride PET coronary uptake in patients with advanced coronary artery disease (CAD)" [87]. ^{18}F-NaF PET has been used to image calcification in coronary arteries, with higher signal detected in foci of microcalcification than in macrocalcification. Uptake of ^{18}F-NaF was previously shown in culprit lesions after MI, and, more recently, a high global ^{18}F-NaF signal has been shown to be associated with a higher risk of MI. These authors compared ^{18}F-NaF PET results with those from calcium scoring in ~300 patients and showed that ^{18}F-NaF PET outperformed calcium scoring for prediction of MI. In addition, they developed a machine learning model that incorporated ^{18}F-NaF PET, clinical, and CT data and showed that these 3 together outperformed either clinical data or clinical data plus CT. This method can be used to upscale or downscale the estimated risk of MI in specific patients. On the left in Figure 2, ^{18}F-NaF signal was seen in the coronary artery in a 49-year-old man, leading to an increase in estimation of risk of MI. On the right, estimation of risk was reduced in a patient with no coronary ^{18}F-NaF signal.

The Cardiovascular Council presents 2 prestigious awards. The Hermann Blumgart Award is the top award and recognizes outstanding scientific contributions to the field and service to the council. At this meeting, the award went to

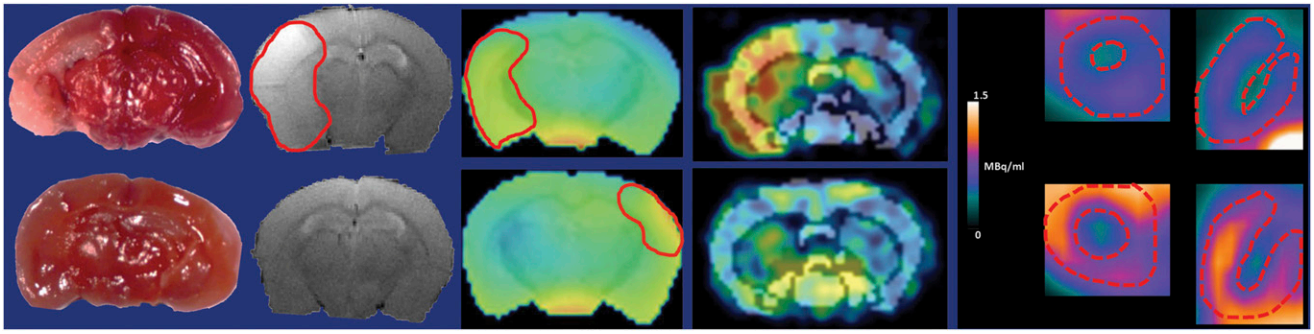

FIGURE 1. Molecular imaging of inflammation in the brain–heart axis after ischemic stroke in 2 murine models. Top row, first 4: Middle cerebral artery occlusion (MCAO) model imaged with triphenyltetrazolium chloride staining, MRI, ^{18}F-GE180 PET, and autoradiography at 7 days after occlusion showed large-size stroke and neuroinflammation. Bottom row, first 4: Model with topical application of a vasoconstrictor, endothelin-1, to cortex evoked limited stroke and neuroinflammation. Larger stroke size led to greater cardiac dysfunction. Far right block: Short- and vertical long-axis cardiac images; top: sham-operated mice at 7 d after surgery; bottom: MCAO model mice at 7 d after surgery. The study expands understanding of brain–heart networking after stroke.

Piotr Slomka, PhD, Professor of Medicine at the Cedars-Sinai Medical Center (Los Angeles, CA) and the David Geffen School of Medicine at the University of California, Los Angeles. The new Outstanding Educator Award recognizes the contribution of cardiovascular educators. The awardee was Diwakar Jain, MD, from Westchester Medical Center (Valhalla, NY).

We had a large number of outstanding abstracts this year on various aspects of nuclear cardiology and molecular imaging. Because of time limitations I have selected a few representative examples and apologize to the authors of important work not reviewed here.

Refining the Practice of Nuclear Medicine

Myocardial Perfusion Imaging. Myocardial perfusion imaging (MPI) is the cardiovascular procedure we perform most often in our laboratories and that in many ways defines the field of nuclear cardiology. This year several innovations in MPI were presented during the meeting. These included refinements to imaging and image analysis protocols and ways to enhance the value of perfusion imaging in patient management. As an example, Arida-Moody et al. from the University of Michigan Health System (Ann Arbor) and INVIA (Ann Arbor, MI, and Ottawa, Canada) reported on "Comparison of weight- and body mass index [BMI]–adjusted dosing for dynamic ^{82}Rb PET myocardial perfusion imaging" [1592]. The BMI-dosing protocol significantly reduced both the frequency and severity of detector saturation, as well as the overall mean ^{82}Rb dose and effective radiation exposure.

Another example of innovations in imaging protocols and image analysis came from Yang et al. from the University of California San Francisco and Yale University (New Haven, CT), who reported on "CT-less attenuation correction in image space using deep learning for dedicated cardiac SPECT: A feasibility study" [223]. Many dedicated cardiac SPECT scanners with cadmium-zinc-telluride (CZT) do not have an integrated CT for attenuation correction. These authors developed a deep learning approach to generate attenuation-corrected SPECT images directly from non-corrected SPECT without undergoing an additional image reconstruction step. The results yielded more uniform images on a segmental basis than non–attenuation corrected images. This can be seen in Figure 3, where the diaphragmatic attenuation artifact is improved with both the CT attenuation correction and the deep learning approach.

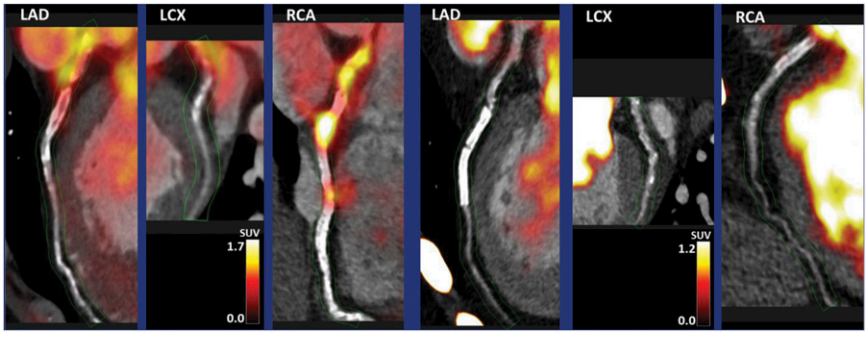

FIGURE 2. Upscaling and downscaling of patient risk with ^{18}F-NaF–based machine learning. Left 3 images, left to right: left anterior descending (LAD), left circumflex (LCX), and right coronary artery (RCA) ^{18}F-NaF PET/CT in a 49-year-old male with coronary microcalcification activity of 10.5. Clinical and CT data alone provided a 1.5% risk estimate of MI (47th percentile). Combining ^{18}F-NaF PET, CT, and clinical data produced a risk estimate of 8% (81st percentile). Right 3 images: corresponding images in a 75-year-old man with no microcalcification activity and a 2.3% clinical plus CT-estimated risk (57th percentile). The addition of ^{18}F-NaF PET downscaled this predictive risk to 1.1% (the 32nd percentile).

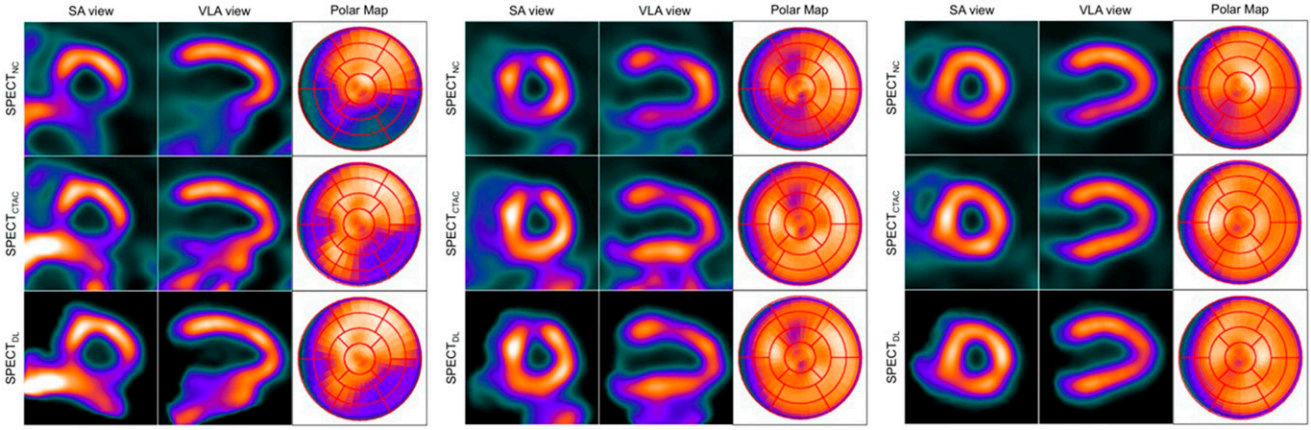

FIGURE 3. CT-less attenuation correction in image space using deep learning for dedicated cardiac SPECT. Examples from 3 subjects in (left to right in blocks) short- and vertical long-axis views and polar maps. Top row: non–attenuation corrected SPECT; middle row: CT–attenuation corrected SPECT; and bottom row deep learning–attenuation corrected SPECT. The deep learning approach yielded more uniform images on a segmental basis than non–attenuation corrected images.

Another deep learning application in MPI analysis came from Otaki (a YIA finalist) et al. from Cedars-Sinai Medical Center (Los Angeles, CA), Israel and Ben Gurion University of the Negev (Beer Sheba Israel), Veterans General Hospital (Taipei, Taiwan), Columbia University Medical Center (New York, NY), Oregon Heart and Vascular Institute (Springfield), University of Ottawa Heart Institute (Canada), University Hospital Zurich (Switzerland), Yale University (New Haven, CT), and Brigham and Women's Hospital (Boston, MA), who reported on "Diagnostic accuracy of deep learning for MPI in men and women with a high-efficiency parallel-hole-collimated CZT camera: Multicenter study" [92]. They used data from the REgistry of Fast Myocardial Perfusion Imaging with NExtgeneration SPECT (REFINE), including 1,160 MPIs from patients with no history of prior CAD and with results from invasive angiography within 6 months of MPI. These authors developed a novel deep learning model that incorporates analysis of raw upright and supine stress polar maps, with specification of sex and BMI. Gradient-weighted class activation mapping was employed to visualize regions contributing to disease prediction on polar maps (Fig. 4). This deep learning model outperformed both total perfusion defect and visual scoring by summed stress score in both men and women. They did find, however, that there are differences in sensitivity between women and men and are continuing to study the reasons for this. These authors concluded that their deep learning approach can be applied clinically on a PC to help readers.

Other examples of presentations on novel analytic advances in perfusion imaging included that of Miller et al. from Cedars-Sinai Medical Center Program (Calgary, Canada, Los Angeles, CA, West Hollywood, CA), Assuta Medical Center (Tel Aviv, Israel), Columbia University Medical Center (New York, NY), Oregon Heart and Vascular Institute (Springfield), University of Ottawa Heart Institute (Canada), University Hospital Zurich (Switzerland), Yale University (New Haven, CT), Cardiovascular Imaging Technologies (Kansas City, MO), and Brigham and Women's Hospital (Boston, MA), who reported that "Quantitation of ventricular morphology provides incremental

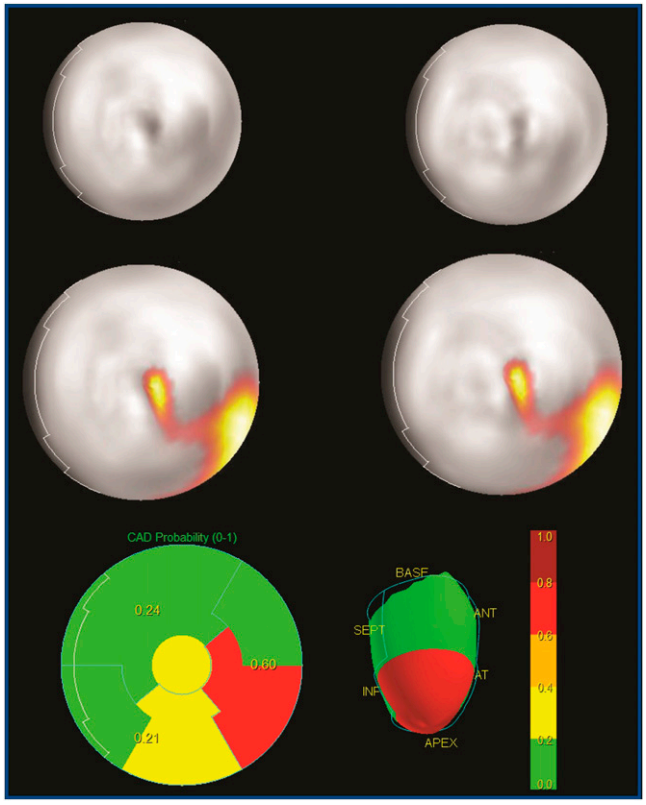

FIGURE 4. Deep learning for myocardial perfusion with a high-efficiency parallel-hole-collimated cadmium-zinc-telluride camera. Top row: Upright and supine raw polar perfusion maps used as input for the deep learning model. Middle row: Upright and supine coronary artery disease (CAD) stress-perfusion attention maps. Bottom row: CAD probability maps as generated by the deep learning model, which outperformed both total perfusion defect and visual scoring by summed stress score in men and women, although sex-based differences in sensitivity were noted.

prognostic utility in patients undergoing SPECT MPI" [660]. They concluded that "changes in ventricular morphology have important prognostic utility and should be included in patient risk estimation following SPECT MPI." Wells and Ruddy from the University of Ottawa Heart Institute (Canada), reported that "Respiratory motion alters measurement of SPECT myocardial blood flow" [654], with respiratory motion causing displacement of the heart by >10 mm in 17% of dynamic scans.

We also heard notable information highlighting the value of MPI. Mannarino et al. from the University Federico II (Naples, Italy) and the Manchester University NHS Foundation Trust (UK) reported on "Prognostic value of coronary vascular dysfunction assessed by hybrid ^{82}Rb PET/CT imaging in patients with resistant hypertension" [640]. They concluded that ^{82}Rb PET/CT in patients with resistant hypertension can help to identify a higher risk of cardiovascular events and could be useful in "guiding alternative potential therapeutic strategies aimed to directly improve myocardial perfusion reserve." Khan et al. from the Marshfield Clinic Health System (WI) and the Hospital of the University of Pennsylvania (Philadelphia) reported that "Risk prediction of coronary flow reserve is strongly influenced by the burden of coronary calcification" [653]. These authors concluded that coronary flow reserve helps to risk stratify patients with coronary artery calcium ≥10.

Imaging Infiltrative Cardiomyopathy and Device and Valve Infection. Imaging of infiltrative cardiomyopathy and of device and valve infection are routinely performed in many nuclear imaging laboratories. The focus has now shifted from proof of principle to refining the ways in which these tests are performed, acquiring quantitative information, and improving accuracy. Several associated innovations were reported this year. As an example, Bukhari et al. from the University of Pittsburgh Medical Center (PA) reported on "Clinical predictors of positive ^{99m}Tc-pyrophosphate scan in patients hospitalized for decompensated heart failure" [659]. At their institution, they found that almost one-third of hospitalized patients with clinically suspected cardiac amyloidosis had final diagnoses of wild-type transthyretin amyloid cardiomyopathy. A history of carpal tunnel syndrome, ECG findings of low QRS voltage, atrioventricular block and left anterior fascicular block, and echocardiographic features of LV hypertrophy and high-grade diastolic dysfunction were prevalent in these patients. Poitrasson-Riviere et al. from INVIA Medical Imaging Solutions (Ann Arbor, MI) and the University of Michigan (Ann Arbor, MI) reported on "Quantitative assessment of inflammatory ^{18}F-FDG PET scans for diagnosis of cardiac sarcoidosis" [650]. They found that "quantification of LV myocardial ^{18}F-FDG activity above blood pool SUV is a reliable method for diagnosis of myocardial inflammation and is associated with worse prognosis."

Other investigators looked at imaging device and valve infection. Abikhzer et al. from the Jewish General Hospital (Montreal, Canada), Health Sciences Centre (Winnipeg, Canada), and the Institut de Cardiologie de Montreal (Canada) reported on "FDG-PET CT for the evaluation of native valve endocarditis" [645]. They found that "the addition of positive ^{18}F-FDG PET/CT as a major criterion in the modified Duke Criteria improved performance of the criteria for diagnosis of patients with native valve endocarditis, particularly in those subjects with possible infectious endocarditis." [645].

Sommerlath Sohns et al. from the Hannover Medical School (Germany) reported that "Inflammatory volume from ^{18}F-FDG PET/CT assists in prognostic assessment of patients with LV assist device (LVAD) infection" [644]. Looking at data from 50 patients with LVAD infections, they quantified the ^{18}F-FDG signal in different components of the device (Fig. 5). They found that patients with high c-reactive protein and high ^{18}F-FDG signal volume on PET had worse outcomes than other groups and suggested

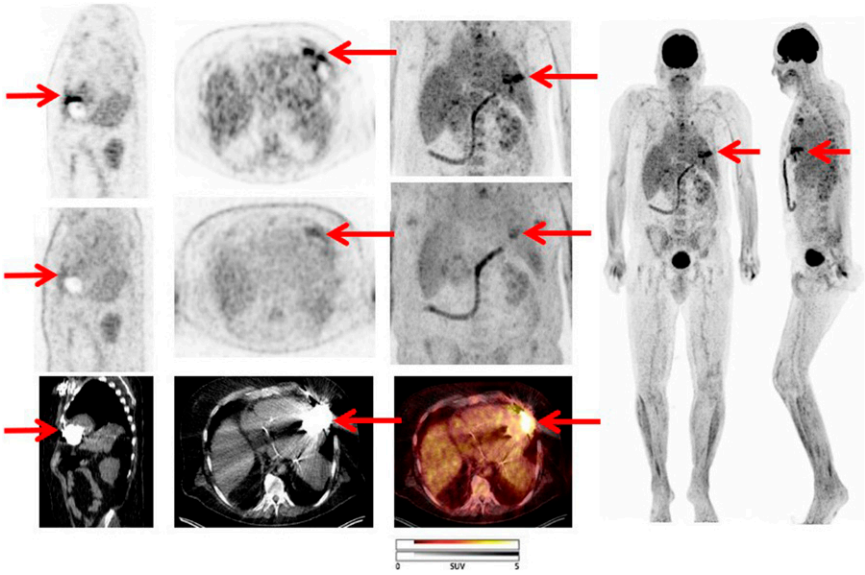

FIGURE 5. Inflammatory volume from ^{18}F-FDG PET/CT in prognostic assessment of patients with left ventricular assist device (LVAD) infection. Example of a patient with LVAD infection. Left to right: Sagittal, axial/transverse, MIP and fusion PET/CT, and MIP coronal/sagittal images. Top to bottom, first 3 columns, attenuation-corrected ^{18}F-FDG PET, non–attenuation corrected ^{18}F-FDG PET, and CT. Patients with high c-reactive protein and high ^{18}F-FDG signal volume on PET had worse outcomes than other groups. This combination of parameters was suggested as a useful way to identify a patient subset at highest risk of adverse outcomes.

this combination of parameters as a useful way to identify a patient subset at highest risk of adverse outcomes.

Expanding the Horizon

Beyond the tests routinely performed in many nuclear laboratories, investigators are introducing new applications and tracers to expand the horizons for molecular imaging in cardiovascular medicine. Some notable examples of these innovations are listed here, spanning from heart failure to aneurysm and calcific aortic valve disease. Examples of research presented on new applications included, among others, Thayumanayan et al. from the All India Institute of Medical Sciences (New Delhi, India), who reported on "Fluorine-18 fluoro-L-dihydroxyphenylalanine (^{18}F-FDOPA) PET-CT in evaluation of cardiac sympathetic innervation in heart failure patients" [648]; Nakahara et al. from the Keio University School of Medicine (Tokyo, Japan), Fukushima Medical University (Japan), Memorial Sloan Kettering Cancer Center (New York, NY), and Mount Sinai (New York, NY), who reported that "The combination of ^{18}F-FDG and ^{18}F-NaF uptake predicts the development of abdominal aortic aneurysm in rat model" [31]; Zadeh et al. from Children's Hospital of Philadelphia (PA), the Perelman School of Medicine at the University of Pennsylvania (Philadelphia), Odense University (Denmark), and Oslo University Hospital (Norway), who reported on "Assessing risk of atherosclerosis in smoldering multiple myeloma patients by means of ^{18}F-sodium fluoride with global assessment" [635]; Diekmann et al. from the Hannover Medical School, Charité Universitätsmedizin Berlin, and the Technische Universität München (all in Germany), who reported that "Clinical imaging of chemokine receptor CXCR4 early after acute MI predicts subsequent ventricular dysfunction and remodeling" [663]; and Farber et al. from the University of Ottawa/University of Ottawa Heart Institute (Canada), who reported on "Multimodality imaging to predict calcific aortic valve disease progression in animal models" [27]. An example of research presented on new tracers was Gali et al. from the University of Oklahoma Health Science Center (Oklahoma City) and Hexakit, Inc. (Oklahoma City, OK), who reported on "Evaluation of ^{18}F-FGA PET/CT for specific imaging of necrotic tissue in a mouse model of coronary artery ligation" [228].

I will highlight here a few of the new applications and tracers that are currently in different stages of development. Woodard et al. from Washington University St. Louis (MO) and the University of California at Santa Barbara reported on "Targeted natriuretic peptide receptor-C (NPR-C) PET/MR imaging of carotid atherosclerosis in humans: Correlation with ex vivo plaque immunohistochemistry (IHC)" [636]. This was a first-in-human study. There is considerable debate on how patients with asymptomatic carotid stenosis should be managed, and molecular imaging may help risk-stratify these individuals. These researchers have developed a nanoparticle radiotracer, ^{64}Cu-CANF-Comb, that targets NPR-C, a molecule expressed on macrophages and smooth muscle cells and is upregulated in atherosclerosis. In 15 patients scheduled for carotid endarterectomy they showed uptake of the tracer in cardiac atherosclerosis on PET/MR imaging (Fig. 6) and were able to characterize the plaque. After carotid endarterectomy and IHC, they identified a significant correlation between the tracer signal and NPR-C expression in the tissue, indicating that they are indeed imaging this target in vivo. Follow up studies should establish whether this approach can be used routinely for risk stratification in carotid stenosis.

Improving risk stratification in abdominal aortic aneurysm (AAA) is another potential novel application of molecular imaging. This is a rapidly advancing field with several innovations introduced this year. Heo et al. from the Washington University School of Medicine (St. Louis, MO) reported on "Assessment of AAA inflammation and rupture prediction with chemokine receptor 2 [CCR2] PET" [23]. They evaluated ^{64}Cu-DOTA-ECL1i, a novel tracer that binds to CCR2, in a rat model of AAA. Their in vivo PET imaging studies showed higher uptake of the tracer in the rat model of AAA than in sham-operated animals at 7 days after surgery (Fig. 7). They showed that the signal was specific, and, of particular note, that the signal was higher in animals that experienced aneurysm rupture than in animals that did not. They concluded that CCR2 PET might be used for growth and/or rupture prediction in AAA.

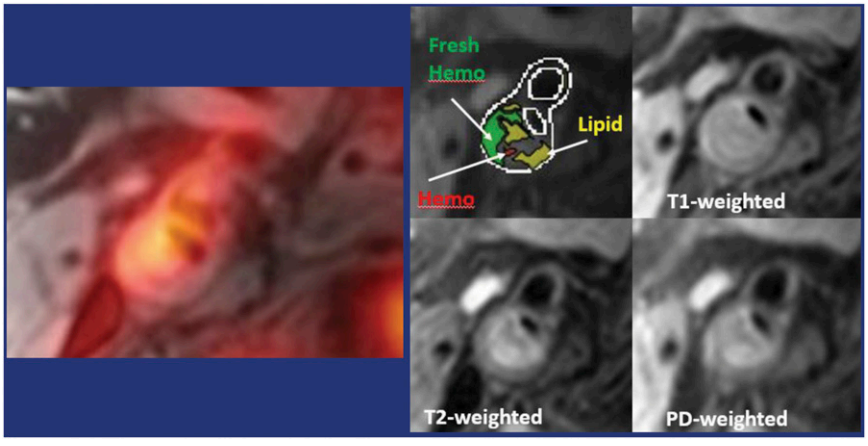

FIGURE 6. Targeted natriuretic peptide receptor-C (NPR-C) PET/MR imaging of carotid atherosclerosis. Fused PET/MR image (left) in a patient with high ^{64}Cu-CANF-Comb PET uptake in the right common carotid artery in a plaque with intraplaque hemorrhage on multiweighted MRI (right images). This first-in-human study correlated the carotid tracer signal with immunohistochemistry-assessed NPR-C expression in carotid endarterectomy tissue, an approach with promise for clinical risk stratification in carotid stenosis.

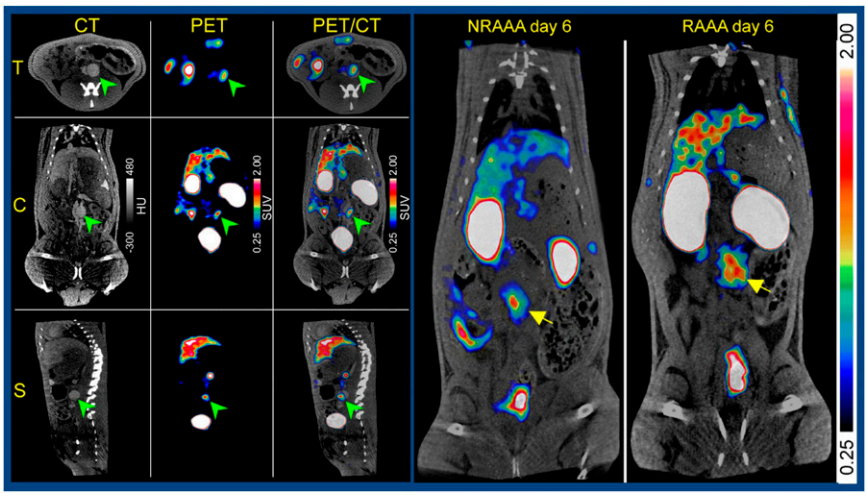

FIGURE 7. Improving risk stratification in abdominal aortic aneurysm (AAA) with chemokine receptor 2 (CCR2) PET. ^{64}Cu-DOTA-ECL1i PET in a rat model of AAA showed tracer binding in AAA [left 3 columns: CT, PET, and PET/CT in (top to bottom) transverse, coronal, and sagittal views]. Imaging at 7 days postsurgery showed higher uptake of the tracer in the AAA rat model than in sham-operated animals. Right 2 images: Tracer uptake in AAAs that subsequently ruptured (right) demonstrated uptake nearly twice that of nonruptured AAAs (left), despite comparable diameters of aneurysms in the 2 models.

Following the same theme, Toczek (a YIA finalist) et al. from the Yale University School of Medicine (New Haven, CT) and the Veterans Affairs Connecticut Healthcare System (West Haven) reported on "Multimodal molecular imaging of phagocytic and proteolytic activity in AAA" [89]. Using a nanoparticulated CT contrast agent in a mouse model of AAA, they were able to detect aortic dilation 5 minutes after contrast administration (Fig. 8). Within 24 hours, uptake of the tracer was evident in the AAA wall. Transmission emission microscopy showed that this nanoparticle localizes in adventitial macrophages, and immunostaining of aneurysm showed a significant correlation between macrophage marker expression and CT signal but not between smooth muscle or endothelial cell markers and CT signal. In addition, a group of animals in this study underwent dual-modality SPECT/CT imaging to

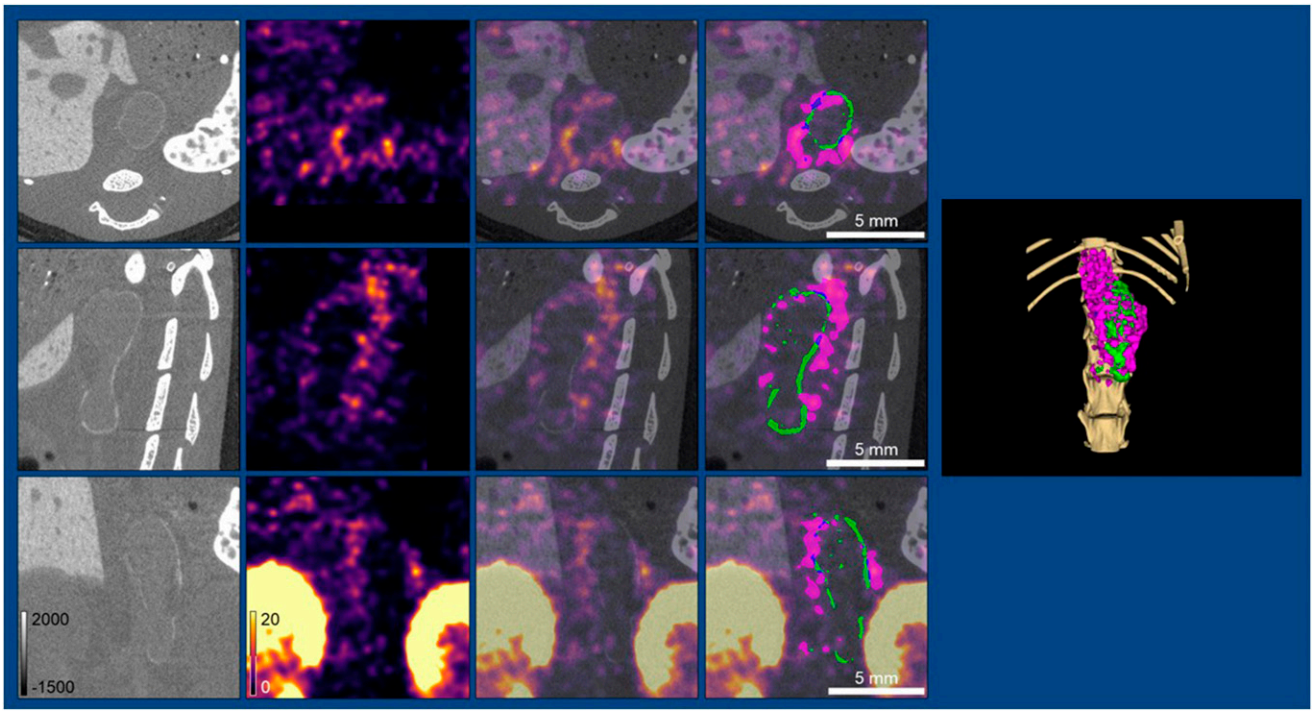

FIGURE 8. Dual-modality SPECT/CT imaging of phagocytic and matrix metalloproteinase (MMP) activity in abdominal aortic aneurysm (AAA). Columns, left to right: CT imaging of phagocytic activity, SPECT imaging of MMP activity, fusion SPECT/CT, and segmentation. Using a nanoparticulated CT contrast agent in this mouse model of AAA, the authors were able to detect aortic dilation 5 minutes after contrast administration and, within 24 hours, uptake of the tracer was evident in the AAA wall. In animals that underwent both CT imaging to detect phagocytic activity and MMP SPECT imaging, both signals were present in the AAA but not necessarily at the same location, indicating distinct patterns of phagocytic activity and MMP-associated proteolytic activity in AAA.

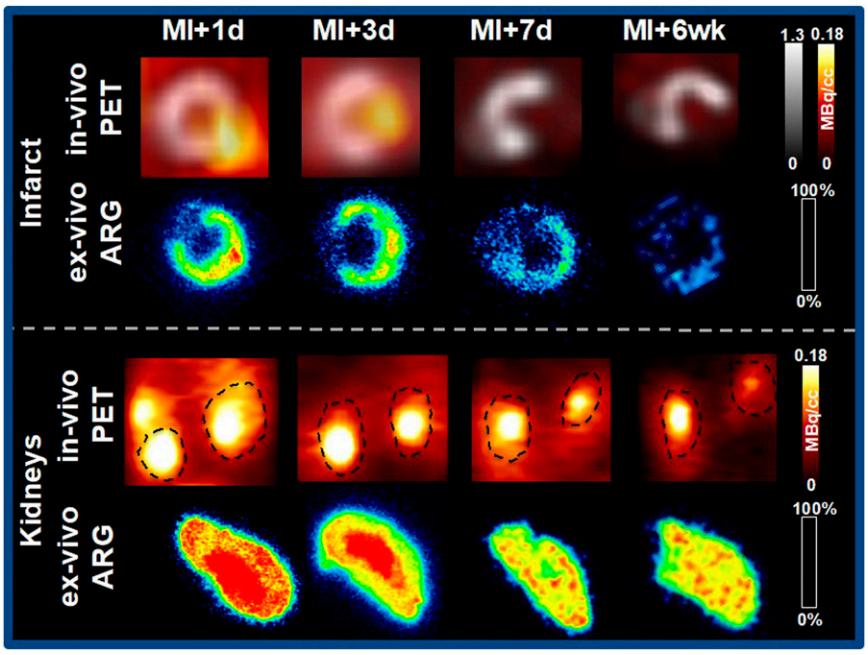

FIGURE 9. Imaging inflammation crosstalk along the cardio–renal axis after myocardial infarction (MI) in a mouse model. Serial ^{68}Ga-pentixafor PET images of chemokine receptor 4 expression at (left to right) 1, 3, and 7 days and 6 weeks after MI showed transient upregulation in the infarct region (top 2 rows, in vivo PET and ex vivo autoradiography) early after MI with, a corresponding increase in renal uptake (bottom 2 rows, in vivo PET and ex vivo autoradiography). Serial ^{68}Ga-pentixafor uptake in the infarct strongly correlated with kidney uptake, suggesting crosstalk between the injured heart and kidneys after MI, which may contribute to adverse outcomes for both organs.

detect phagocytic activity with CT and matrix metalloproteinase activity with SPECT. Both signals localized in aneurysm but did not exactly co-localize. Distinct uptake patterns suggested that the 2 processes are not overlapping but, instead, are complementary.

Accelerating Scientific Discovery

Other investigators took advantage of molecular imaging to accelerate scientific discovery. Werner et al. from the Hannover Medical School and the Technische Universität München (Garching; both in Germany) reported on "Imaging inflammation crosstalk along the cardio–renal axis after acute MI" [28]. Using ^{68}Ga-pentixafor, a tracer that targets the chemokine receptor CXCR4 found in inflammation, they imaged a large group of mice at different time points after coronary artery ligation to induce MI. Serial ^{68}Ga-pentixafor PET images of CXCR4 expression revealed transient upregulation in the infarct region early after MI with a corresponding increase in renal uptake (Fig. 9). This signal declined proportionally in both organs over 6 weeks. In addition, the ^{68}Ga-pentixafor uptake in the infarct strongly correlated with

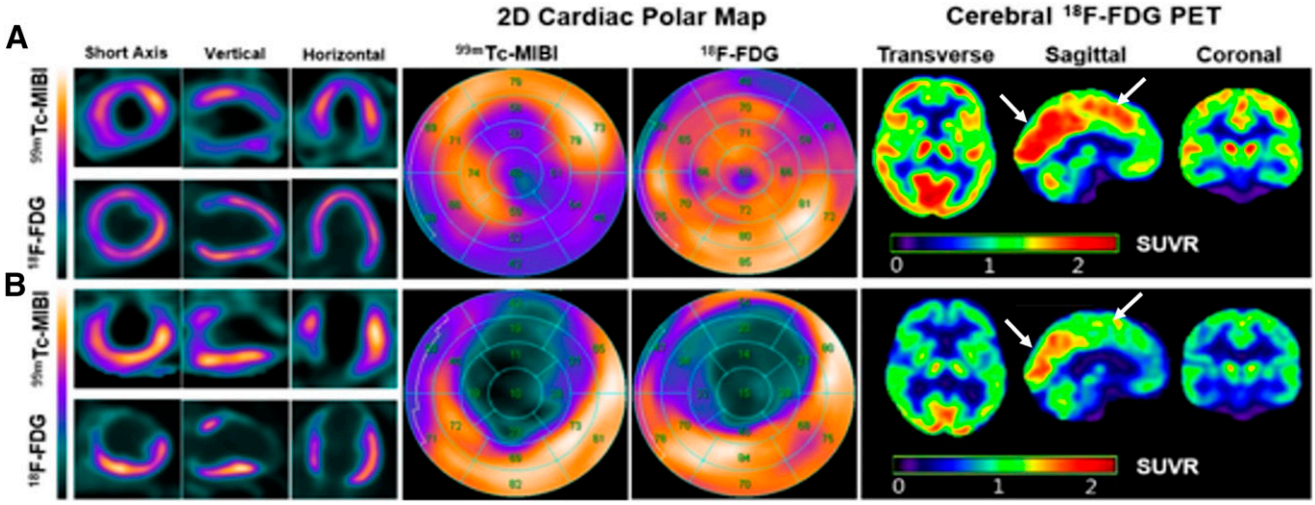

FIGURE 10. Gated SPECT myocardial perfusion and cardiac/cerebral ^{18}F-FDG PET imaging in 2 patients with heart failure, highlighting differences found in various groups in the study. (A) ^{99m}Tc-sestamibi SPECT (top row) and ^{18}F-FDG PET of the heart, 2D cardiac polar maps, and cerebral ^{18}F-FDG PET/CT images acquired in a 41-year-old man with New York Heart Association (NYHA) stage IV disease, 42% left ventricular (LV) hibernating myocardium (HM), 3% LV scar, LV ejection fraction (LVEF) of 20%, end-diastolic volume (EDV) of 258 mL. B. Bottom rows of corresponding imaging in a 42-year-old man with NYHA stage III disease, 3% LV HM, 57% LV scar, LVEF of 15%, EDV of 363 mL. Overall, cerebral metabolism in the whole brain was reduced but maintained in cognition-related frontal areas in heart failure patients with HM and moderately impaired LV function.

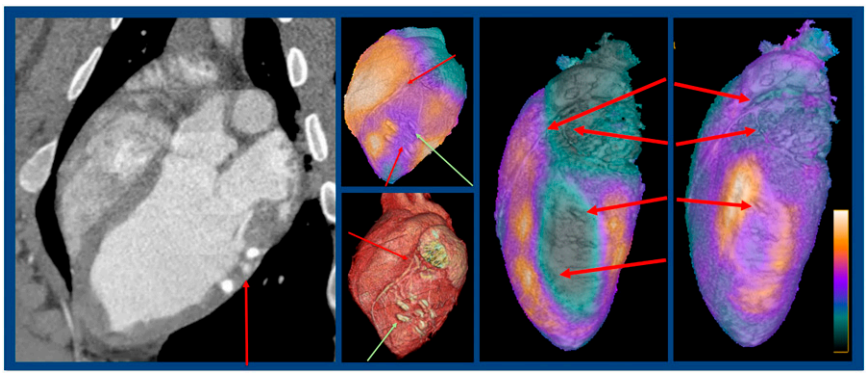

FIGURE 11. Intramyocardial hydrogel delivery after myocardial infarction (MI) in a pig model of induced MI. Left to right: CT imaging tracked the delivery of the hydrogel (which contained a contrast agent); SPECT/CT ^{201}Tl imaging identified the infarct area, and, along with 3D CT, indicated that the hydrogel was delivered to the right place; and ex vivo imaging with SPECT/CT with ^{201}Tl or ^{99m}Tc-maraciclatide, an $\alpha_v\beta_3$ integrin–targeted tracer, showed that the latter tracer localized within the infarct area. Intramyocardial delivery of hydrogel post-MI resulted in increased integrin activation in the MI region and decreased left ventricular remodeling.

kidney uptake. Of note, the kidney PET signal at 7 days post-MI predicted cardiac functional decline at 6 weeks post-MI in mice with severely impaired EF (<30%) but not with modestly impaired ejection fraction (≥30%). This suggests crosstalk between the injured heart and the kidneys after MI, which may contribute to adverse outcomes for both organs.

Following the same theme, this time in humans, Yun et al. from the Beijing Anzhen Hospital (China), the Chinese Academy of Sciences (Beijing, China), the Medical University of Vienna (Austria), and the David Geffen School of Medicine University of California Los Angeles reported on "Assessment of the metabolic heart–brain axis with cardiac and brain ^{18}F-FDG PET/CT imaging in patients with heart failure" [91]. Heart failure may be associated with cognitive impairment. The authors sought to evaluate a potential association between the brain and heart metabolic activity in patients with heart failure. Their patients with ischemic cardiomyopathy underwent ^{99m}Tc-sestamibi SPECT/CT MPI as well as cardiac and cerebral ^{18}F-FDG PET/CT. Participants were categorized based on the extent of hibernating myocardium and EF values, and these were compared with data from healthy/normal volunteers. A significant difference in whole-brain SUV was observed among the patient subgroups and volunteers, most notably between the normal group and the group with hibernating myocardium <10% LV. Differences were also noted in different regions of the brain between the study groups. Figure 10 shows examples of 2 subjects with different extents, high and low, of hibernating myocardium based on ^{18}F-FDG PET and MIBI SPECT, with differing levels of ^{18}F-FDG signal in the brain. Overall, cerebral metabolism in the whole brain was reduced but maintained in cognition-related frontal areas in heart failure patients with hibernating myocardium and moderately impaired LV function.

Changing direction, Melvinsdottir et al. from Yale University (New Haven, CT) and the University of Pennsylvania (Philadelphia) reported that "Intramyocardial hydrogel delivery post MI results in increased integrin activation and reduction in LV modeling" [90]. The work was conducted in a pig model of induced MI. As seen in Fig. 11, the delivery of the hydrogel (which contained a contrast agent) was tracked by CT, and SPECT/CT ^{201}Tl imaging identified the infarct area, and, along with 3D CT, indicated that the hydrogel was indeed delivered to the right place. Ex vivo imaging with ^{99m}Tc-maraciclatide, an $\alpha_v\beta_3$ integrin–targeted tracer, showed this agent localized within the infarct area, and gamma well counting showed higher $\alpha_v\beta_3$ tracer uptake in animals with MI and hydrogel compared to MI alone. Intramyocardial delivery of hydrogel post-MI resulted in increased integrin activation in the MI region and decreased LV remodeling. The authors concluded that multimodality imaging is a feasible approach for guiding delivery and monitoring the effects of a therapeutic hydrogel.

Summary

The presentations reviewed here covered a broad range of topics representing the state of the art in nuclear and molecular imaging in cardiology, including refining the practice of nuclear cardiology, addressing diagnostic gaps and novel applications of molecular imaging, and advancing scientific discovery. Ongoing improvements in MPI increase its value for patient care, and novel molecular imaging approaches continue to be incorporated into patient management. Emerging molecular imaging approaches may address a number of existing diagnostic gaps in cardiovascular medicine. Molecular imaging is advancing basic cardiovascular research beyond what is possible with traditional laboratory techniques. This year's SNMMI Annual Meeting was held virtually, in a time of global uncertainty. The quality of abstracts presented at the meeting and the dedication of the scientists and clinicians who shared their work here constitute a testimony to the vitality and prospects of our field in improving patient care and advancing science.